Selective photodeposition of zinc nanoparticles on the core of a single-mode optical fiber

J. G. Ortega-Mendoza,[1,*] F. Chávez,[2] P. Zaca-Morán,[2] C. Felipe,[3] G. F. Pérez-Sánchez,[2] G. Beltran-Pérez,[1] O. Goiz,[4] and R. Ramos-Garcia[5]

[1]*Facultad de Ciencias Físico-Matemáticas, Universidad Autónoma de Puebla, CP 72320, Puebla, Pue., México.*
[2]*Departamento de Fisicoquímica de Materiales, Universidad Autónoma de Puebla, CP 72050, Puebla, Pue., México.*
[3]*Departamento de Biociencias e Ingeniería, Centro Interdisciplinario de Investigaciones y Estudios Sobre Medio Ambiente y Desarrollo del Instituto Politécnico Nacional, CP 07340, México D. F., México.*
[4]*Departamento de Ingeniería Eléctrica, Centro de Investigación y de Estudios Avanzados del Instituto Politécnico Nacional, CP 07000, México D.F., México.*
[5]*Departamento de Óptica, Instituto Nacional de Óptica y Electrónica, CP 72840, Tonantzintla, Pue., México.*
[*]*jgaomen@hotmail.com*

Abstract: An experimental and theoretical study about selective photodeposition of metallic zinc nanoparticles onto an optical fiber end is presented. It is well known that metallic nanoparticles possess a high absorption coefficient and therefore trapping and manipulation is more challenging than dielectric particles. Here, we demonstrate a novel trapping mechanism that involves laser-induced convection flow (due to heat transfer from the zinc particles) that partially compensates both absorption and scattering forces in the vicinity of the fiber end. The gradient force is too small and plays no role on the deposition process. The interplay of these forces produces selective deposition of particles whose size is directly controlled by the laser power. In addition, a novel trapping mechanism termed convective-optical trapping is demonstrated.

OCIS codes: (060.2390) Fiber optics, infrared; (350.5340) Photothermal effects; (350.4855) Optical tweezers or optical manipulation; (140.7010) Laser trapping.

References and links

1. H. Gleiter, "Nanostructured materials: basic concepts and microstructure," Acta Mater. **48**(1), 1–29 (2000).
2. I. O. Sosa, C. Noguez, and R. G. Barrera, "Optical properties of metal nanoparticles with arbitrary shapes," J. Phys. Chem. B **107**(26), 6269–6275 (2003).
3. R. F. Haglund, Jr., L. Yang, R. H. Magruder III, C. W. White, R. A. Zuhr, L. Yang, R. Dorsinville, and R. R. Alfano, "Nonlinear optical properties of metal-quantum-dot composites synthesized by ion implantation," Nucl. Instrum. Meth. B **91**(1-4), 493–504 (1994).
4. H. Amekura, H. Kitazawa, N. Umeda, Y. Takeda, and N. Kishimoto, "Nickel nanoparticles in silica glass fabricated by 60 keV negative-ion implantation," Nucl. Instrum. Meth. B **222**(1-2), 114–122 (2004).
5. H. Amekura, N. Umeda, K. Kono, Y. Takeda, N. Kishimoto, Ch. Buchal, and S. Mantl, "Dual surface plasmon resonances in Zn nanoparticles in SiO_2: an experimental study based on optical absorption and thermal stability," Nanotechnology **18**(39), 1–6 (2007).
6. Y. Chu, E. Schonbrun, T. Yang, and K. B. Crozier, "Experimental observation of narrow surface plasmon resonances in gold nanoparticle arrays," Appl. Phys. Lett. **93**(18), 181108 (2008).
7. I. Tanahashi, H. Inouye, and A. Mito, "Femtosecond nonlinear optical properties of Au/SiO_2 composite thin films prepared by a sputtering method," Jpn. J. Appl. Phys. **42**(Part 1, No. 6A), 3467–3468 (2003).
8. N. Pincon-Roetzinger, D. Prot, B. Palpant, E. Charron, and S. Debrus, "Large optical Kerr effect in matrix-embedded metal nanoparticles," Mater. Sci. Eng. C **19**(1-2), 51–54 (2002).
9. M. Born and E. Wolf, Principles of Optics (Cambridge University Press 1999).
10. A. Ashkin, J. M. Dziedzic, J. E. Bjorkholm, and S. Chu, "Observation of a single-beam gradient force optical trap for dielectric particles," Opt. Lett. **11**(5), 288–290 (1986).
11. K. Svoboda and S. M. Block, "Optical trapping of metallic Rayleigh particles," Opt. Lett. **19**(13), 930–932 (1994).
12. M. Dienerowitz, M. Mazilu, and K. Dholakia, "Optical manipulation of nanoparticles: a review," J. Nanophotonics **2**(1), 1–32 (2008).

#175523 - $15.00 USD Received 5 Sep 2012; revised 15 Oct 2012; accepted 16 Oct 2012; published 8 Mar 2013

13. R. R. Agayan, F. Gittes, R. Kopelman, and C. F. Schmidt, "Optical trapping near resonance absorption," Appl. Opt. **41**(12), 2318–2327 (2002).
14. A. Constable, J. Kim, J. Mervis, F. Zarinetchi, and M. Prentiss, "Demonstration of a fiber-optical light-force trap," Opt. Lett. **18**(21), 1867–1869 (1993).
15. J. W. Nicholson, R. S. Windeler, and D. J. Digiovanni, "Optically driven deposition of single-walled carbon-nanotube saturable absorbers on optical fiber end-faces," Opt. Express **15**(15), 9176–9183 (2007).
16. K. Kashiwagi, S. Yamashita, and S. Y. Set, "Optically manipulated deposition of carbon nanotubes onto optical fiber end," Jpn. J. Appl. Phys. **46**(40), L988–L990 (2007).
17. Z. Luo, M. Zhou, J. Weng, G. Huang, H. Xu, C. Ye, and Z. Cai, "Graphene-based passively Q-switched dualwavelength erbium-doped fiber laser," Opt. Lett. **35**(21), 3709–3711 (2010).
18. L. Ming-Shan and Y. Chang-Xi, "Laser-Induced silver nanoparticles deposited on optical fiber core for surface-enhanced Raman scattering," Chin. Phys. Lett. **27**(4), 044202 (2010).
19. T. Liu, X. Xiao, and C. Yang, "Surfactantless Photochemical deposition of gold nanoparticles on an optical fiber core for surface-enhanced Raman scattering," Langmuir **27**(8), 4623–4626 (2011).
20. R. S. Taylor and C. Hnatovsky, "Trapping and mixing of particles in water using a microbubble attached to an NSOM fiber probe," Opt. Express **12**(5), 916–928 (2004).
21. D. Braun and A. Libchaber, "Trapping of DNA by thermophoretic depletion and convection," Phys. Rev. Lett. **89**(18), 188103 (2002).
22. E. Ehrenhaft, "On the physics of millionth of centimeters," Phys. Z. **18**, 352–368 (1917).
23. R. Pimentel-Domínguez, J. Hernández-Cordero, and R. Zenit, "Microbubble generation using fiber optic tips coated with nanoparticles," Opt. Express **20**(8), 8732–8740 (2012).
24. E. Vela, M. Hafez, and S. Régnier, "Laser-induced thermocapillary convection for mesoscale manipulation," Int. J. of Optomechatronics **3**(4), 289–302 (2009).
25. M. Dienerowitz, M. Mazilu, P. J. Reece, T. F. Krauss, and K. Dholakia, "Optical vortex trap for resonant confinement of metal nanoparticles," Opt. Express **16**(7), 4991–4999 (2008).
26. Y. Harada and T. Asakura, "Radiation forces on a dielectric sphere in the Rayleigh scattering regime," Opt. Commun. **124**(5-6), 529–541 (1996).
27. D. Marcuse, *Light Transmission Optics* (Van Nostrand Reinhold, 1972), Chap. 6.
28. C. F. Bohren and D. R. Huffman, *Absorption and Scattering of Light by Small Particles* (Wiley, 1983), Chap. 4.
29. M. P. Silverman, *Waves and Grains* (Princeton U.P., 1998), Chap. 13.
30. http://omlc.ogi.edu/software/mie/
31. L. A. Spielman and S. K. Friedlander, "Role of the electrical double layer in particle deposition by convective diffusion," J. Colloid Interface Sci. **46**(1), 22–31 (1974).

1. Introduction

Nanoparticles have attracted much attention due to their unique optical, mechanical and chemical properties compared with those of the same bulk material. These properties can be tuned by controlling their size and shape [1, 2]. Metallic nanoparticles are especially interesting due to their ultrafast optical response [3], superparamagnetism [4], surface plasmon resonance [5, 6], and large optical nonlinearities [7, 8] among others. Optical manipulation of nanoparticles has been become an important research area because of its potential applications in medicine and other technological fields. Trapping and manipulation of dielectric nanoparticles is more challenging than trapping of dielectric microparticles due to the optics diffraction limit [9], the high beam intensity and the small volume of the nanoparticles [10]. Metallic nanoparticles are even harder to trap due to the appearance of resonant excitation of free electrons in the metal particle coupled to light (plasmons). The optical properties of the metallic particles vary drastically around the plasmon resonant frequency. Thus, for example, optical trapping of metal nanoparticles is possible far from plasmon resonance [11, 12], nevertheless, near plasmon resonance absorption dominates, and particles are repelled from the beam [13]. On the other hand, optical trapping and manipulation of nanoparticles with pigtailed single optical fibers has shown to be an attractive option due to its simplicity and stability [14]. Normal optical fibers can be a useful and simple tool for depositing organic nanostructures (graphene or single-wall carbon nanotubes) on the fiber output end. The optical fiber end with deposited particles can be used as saturable absorber in optical fiber laser cavities [15–17]. Even more, fiber optical tweezers have been used not only for depositing but also for growing silver and gold nanoparticles through photo-reduction techniques [18, 19].

#175523 - $15.00 USD Received 5 Sep 2012; revised 15 Oct 2012; accepted 16 Oct 2012; published 8 Mar 2013

In this article, we report an experimental and theoretical study of the selective photodeposition of zinc nanoparticles onto a single-mode optical fiber end. A near infrared light is employed, where the absorption and scattering forces are much larger than the gradient force even for very small nanoparticles and thus deposition of metal particles should not occur. However, in this work we show that the laser beam induces convection current flow (due to the heat transfer from hot zinc particles) of the liquid directed towards the fiber end, and the absorption and scattering forces partially compensate the Stokes force for certain particle size. Since absorption, scattering and Stokes forces are all dependent on the particle volume and power beam, a mechanism for selecting the particle size deposited on the core of the optical fiber end is set by the interaction of these forces. It is worth to mention that the photodeposition mechanism proposed in this work is completely different to other mechanism of accumulation based on thermocapillary or thermophoresis [20, 21].

2. Experiment

In our experiment, we used a temperature-stabilized single-mode optical fiber laser emitting at λ = 980 nm (Mod. PL980P330J from Thorlabs). The core diameter is ~8.2 μm and the cladding diameter is 125 μm (see Fig. 1). A power meter (Mod. PM20 from Thorlabs), was used to monitor the output power. The optical fiber was prepared by removing the coating, cleaving it and placing it into a solution of isopropyl alcohol and zinc particles as shown in Fig. 1. A cylindrical cell of 1.5 cm in diameter and 7 cm height is used. The cell was filled to ~90% of its capacity. The typical distance from solution free surface to fiber end was approximately 2 cm and the distance from the fiber end to the container bottom was about 4 cm, so the beam spot at the bottom is ~6 mm (Rayleigh distance ~80 μm). The solution was prepared by mixing 8 cc of isopropyl alcohol and 10 mg of zinc powder and then homogenized using an ultrasonic bath from 10 to 15 minutes. Although the solution was homogenized, large clusters of particles could easily be seen by the naked eye.

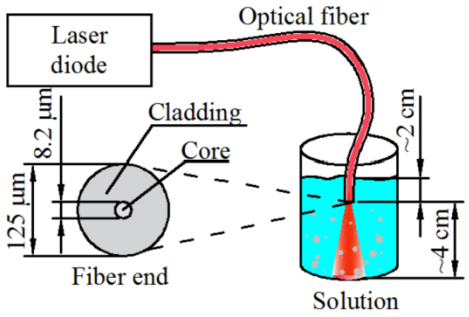

Fig. 1. Experimental setup for depositing Zn nanoparticles onto optical fiber end.

Figure 2(a) shows the morphology of the zinc particles used in this experiment obtained with a scanning electron microscope (TESCAN SEM Vega TS-5136SB). The smallest particle size could not be resolved by our microscope, however, a large particle's size distribution ranging from a few nanometers up to micrometers in diameter is observed. By using X-ray diffraction (PANALYTICAL X´Pert Pro MRD XL), it was confirmed that these particles consist of zinc, however a small signal from ZnO was also detected due to the natural oxidation of zinc (Fig. 2(b)). The shape of zinc particles is quite symmetric and for the purposes of the present work will be assumed to have a spherical shape.

#175523 - $15.00 USD Received 5 Sep 2012; revised 15 Oct 2012; accepted 16 Oct 2012; published 8 Mar 2013

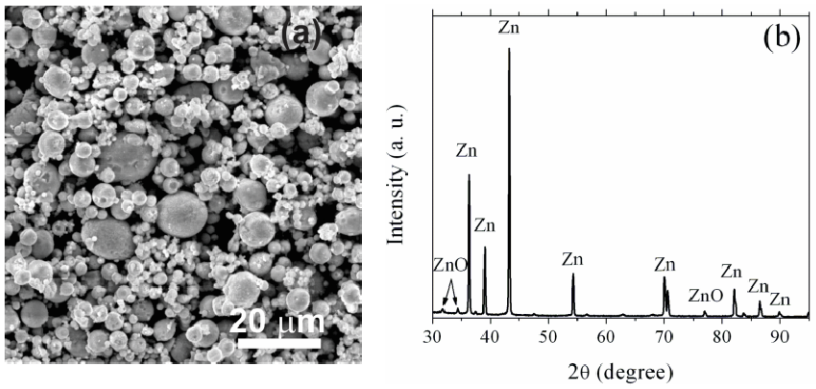

Fig. 2. a) SEM micrograph of zinc powder and the b) corresponding XRD spectrum, confirming the metallic structure of the particles.

3. Results

Figure 3 show images of the optical fiber end obtained under several conditions using a SEM. Figure 3(a) shows that practically no particle deposition is obtained if the laser is off even if the fiber was immersed for long periods of time (15 min). Figure 3(b), 3(e) shows that deposition of the particles occurs once the laser is on, and remain there after the laser is turned off. The amount of deposited particles depends on the beam power and the immersion time of the optical fiber into the solution, while their sizes are related only to the beam power. We observed that there is a threshold power of ~5 mW where practically no particles are deposited even if the immersion time is up to 15 minutes. However, as the power increases above the threshold particles begin to deposit on optical fiber end. Particles are deposited preferably around the fiber core, although some particles are deposited on the fiber cladding. Figure 3(c) shows a close up of Fig. 3(b) around the fiber core. Notice that much smaller particles are deposited on the fiber core (<1 μm in diameter) and larger large particles (≤5 μm in diameter) are deposited around the core. At higher power (50 mW), nanoparticles are deposited just on the core of the optical fiber (Fig. 3(d)). Again, Fig. 3(e) is a close up of the fiber core, indicating that nanoparticles no larger than 100 nm are deposited. Thus, our experimental results indicate that deposition of nanoparticles on core of the optical fiber is an optically activated process. What is more, the deposited particles size is controlled by the beam power. This selective process, could in principle, by used to sort nanoparticles from microparticles or even nanoparticles. Due to the limited power of our laser system and resolution of our SEM, we could not determine the lower limit of deposition.

Figure 4 shows a side-view of fiber end immersed in the colloidal solution (visible on the top central part of the figure). Large clusters of zinc particles are clearly visible by the naked eye as dark spots. When the laser was turned on strong convection currents were observed due to alcohol heating by energy transfer from the hot zinc particles. Particles move upwards, in opposite direction to the beam propagation since the hotter region is confined to the beam volume. It must be pointed out that particles move on the whole volume of the solution and not only on the illuminated volume. The convection currents move upwards and downwards along the wall's container. The same behavior is observed if the solution is replaced by a homogenous absorbing solution. This observation indicates that thermophoresis is ruled out as responsible of the particle movement [22]. Using imaging processing, the speed of a few particle clusters within the illumination cone and in close proximity to the fiber end (visual field shown in Fig. 4) was determined as v_s ~77.6 μm/s for 5 mW laser power and 220.3 μm/s for 50 mW laser power.

#175523 - $15.00 USD Received 5 Sep 2012; revised 15 Oct 2012; accepted 16 Oct 2012; published 8 Mar 2013

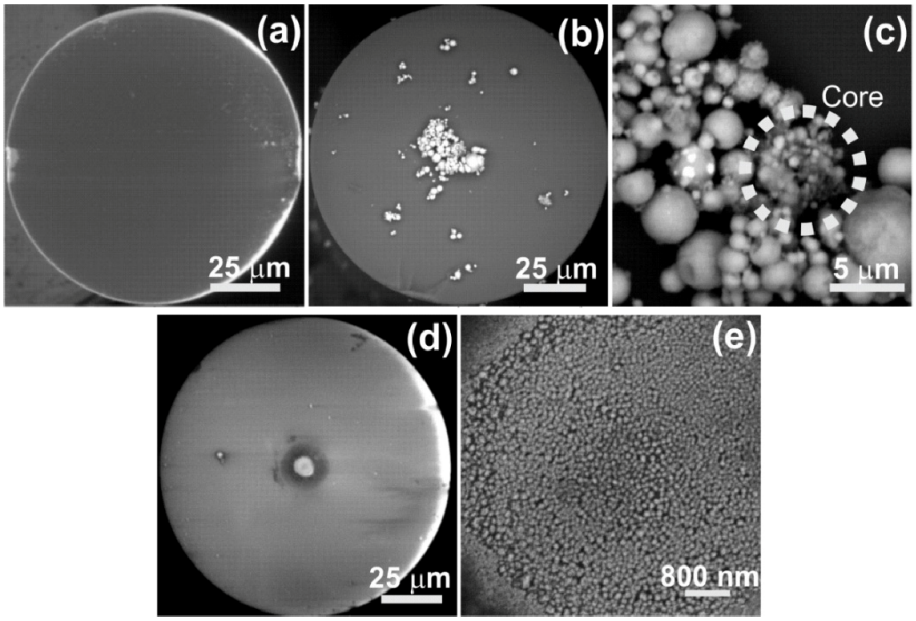

Fig. 3. Images of the optical fiber end obtained with a SEM. a) Optical fiber was immersed into solution for up to 15 minutes with laser light off, b) laser was turned on for 180 seconds and power = 5 mW, c) closer view of b) around the fiber core, d) laser was turned on for 60 seconds and P = 50 mW, e) closer view of the fiber core showed in d).

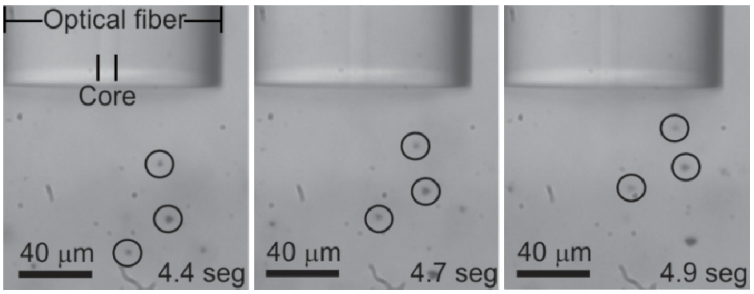

Fig. 4. Consecutive frames show that particles move in opposite direction to the beam propagation. Circles indicate the position of the clusters at different frames (P = 5 mW).

Figure 5(a) is a real-time movie of convection currents to show its spatial extent considering 1 mg of zinc powder dissolved in alcohol and a laser power of 10 mW. It can be observed that zinc particles move upwards in opposite direction to the beam propagation. If the optical fiber is pointing up now, the convection current does not change direction as expected. It is important to note that no deposition occurs under these conditions since scattering and absorption forces point in the same direction.

The flow velocity over the whole field of view was measured by particle tracking using a 100 fps camera. Figure 5(a) shows flow patterns indicated by dotted lines; these indicate the trajectories of the particles when the laser is turned on. The particle velocities outside the beam for two concentrations (1 and 10 mg) are shown in Fig. 5(b). One can see that the steady-state velocity is reached within the first 30 sec and its magnitude does not change appreciable over 3 mins of observation regardless the amount of zinc particles in the solution. Below the threshold power, heating is not enough to establish convective currents with sufficient force to overcome the optical forces, therefore the photodeposition does not occurs. Note that the velocities within the beam (and near to the fiber end) are at least an order of

#175523 - $15.00 USD Received 5 Sep 2012; revised 15 Oct 2012; accepted 16 Oct 2012; published 8 Mar 2013

magnitude smaller than those outside the beam because scattering and absorption forces point in the opposite direction.

Once particles are deposited, they strongly absorb the laser light producing a heat source at the fiber tip. The velocity of the particles not only decreases but its spatial distribution is greatly altered around fiber end since the heat source changes from a cone shape to almost single-point source. If laser power is high enough boiling of isopropyl alcohol is possible, confirmed by the formation of vapor bubbles. The size of bubbles is controlled with the laser power, which in turns, determine the evaporation rate. If this is sufficiently high, cavitation bubbles maybe produced [23] and upon bubble collapse the particles are expelled from the core.

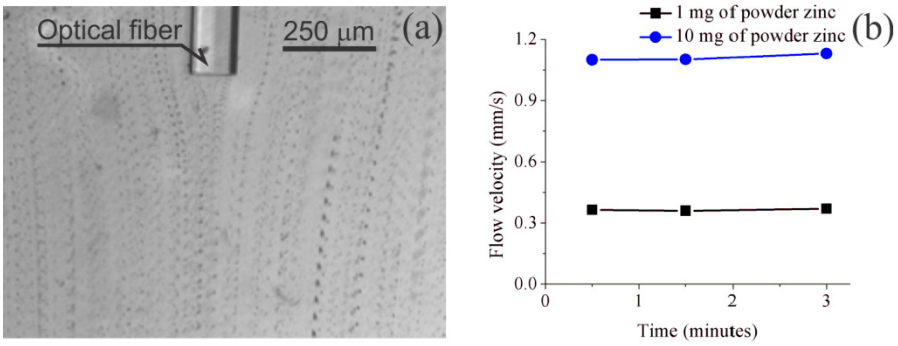

Fig. 5. a) Velocity field illustrating the motion of particles obtained from a real-time movie of convection currents (Media 1). b) Flow velocity as determined by particle tracking for two concentrations using a power of 10 mW.

4. Discussion

When a laser heats up a solution two types of convection currents arise: free convection (also known as Rayleigh convection) and Marangoni convection (also known as thermocapillary). Both types of convection are described by a dimensionless number: i) Rayleigh number *Ra* and ii) Marangoni number *Ma*. For thin cells (<1mm), the Marangoni convection dominates, while for thicker (and larger) cells, the Rayleigh convection dominates [23]. In our experiments, the dimension of our cylindrical cell is 1.5 cm in diameter and 7 cm height (typically filled to 90% of its capacity). For modest temperature difference between hot and cold region (9-40 °C in our experiments), the Rayleigh number (~10^5) easily exceeds the critical Rayleigh number ($Ra_{critical}$~1700) [24]. So, under our experimental conditions, free convection is the mechanism of liquid (and particle) displacement. As mentioned before, thermophoresis is ruled out because particles move not only inside the beam but also outside. Thus, the convection currents will drag the particles at the same speed as the liquid in the vicinity of the fiber regardless of their size. Particles will experience a drag force given by the Stokes force. To the best of our knowledge, free convection currents have not been considered so far as a part of the deposition and trapping mechanism. In order to calculate the Stokes force, we will assume as a first approximation two facts; that all particles move at the same speed (near to the fiber end) and that all particles are spherical. Hence, the force exerted on these particles would be given by the Stokes law:

$$\boldsymbol{F}_{Stokes} = 6\pi\psi R v_s, \qquad (1)$$

where ψ is the dynamic viscosity of host liquid media (dynamic viscosity of isopropyl alcohol $\psi = 0.00196$ Ns/m^2) and v_s is the particle velocity in the vicinity of the fiber end.

Figure 3(a) shows that particle deposition on the optical fiber does not occur in absence of laser light, i.e. is a light-activated process. Figure 6 shows a scheme of the proposed model

#175523 - $15.00 USD Received 5 Sep 2012; revised 15 Oct 2012; accepted 16 Oct 2012; published 8 Mar 2013

and the forces involved in the photodeposition process: gradient force ($\boldsymbol{F}_{grad}$), absorption ($\boldsymbol{F}_{abs}$) and scattering ($\boldsymbol{F}_{scat}$) forces (directed along the beam propagation) and Stokes force ($\boldsymbol{F}_{Stokes}$) (upwards convection current). The net force exerted on a particle is given by Eq. (1)

$$\boldsymbol{F}_{net} = \boldsymbol{F}_{abs} + \boldsymbol{F}_{scat} + \boldsymbol{F}_{Stokes} + \boldsymbol{F}_{grad}. \quad (2)$$

The expressions for scattering and absorption forces are [25]:

$$\boldsymbol{F}_{grad} = \frac{1}{2}\alpha'(\omega)\nabla E^2, \quad (3)$$

$$\boldsymbol{F}_{scat} = \frac{n}{c}\boldsymbol{I}(r)C_{scat}, \quad (4)$$

$$\boldsymbol{F}_{abs} = \frac{n}{c}\boldsymbol{I}(r)C_{abs}, \quad (5)$$

where $\alpha(\omega) = \alpha'(\omega) + i\alpha''(\omega)$ is the particle complex polarisability, c is the speed of light, $\boldsymbol{I}(r)$ is the beam intensity, n the refractive index of the host medium, and C_{scat} and C_{abs} are the scattering and absorption cross-section, respectively, and may be calculated with Mie or Rayleigh theory depending on the size of the particles.

The intensity distribution of the electric field at the fiber end (considering the zeroth-order approximation) is expressed by a Gaussian distribution [26, 27]:

$$\boldsymbol{I}(r) = \left(\frac{2P}{\pi w_0^2}\right)\frac{k^2 w_0^4}{4z^2 + \left(kw_0^2\right)^2} exp\left[-\frac{2kw_0\left(x^2+y^2\right)}{4z^2 + \left(kw_0^2\right)^2}\right], \quad (6)$$

Where P is the beam power, k denotes the wave vector of the light in vacuum, w_0 is the beam waist and (x, y, z) represent the spatial coordinates with + z as the propagation direction.

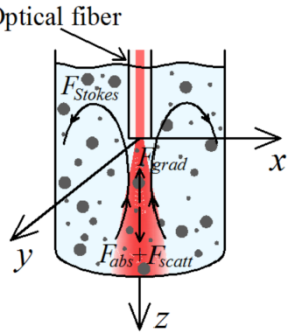

Fig. 6. Schematic representation of the proposed model. Light is propagating along + z axis. The scattering and absorption forces are directed along the + z axis while the Stokes force is directed in the opposite direction.

Basically, there are two methods for calculating light scattering: Rayleigh and Mie approximations. The former one is applicable to particles whose size is much smaller than the wavelength of the light used for optical trapping (Rayleigh particles, $R<\lambda/20$ ~50 nm) while the latest one is not limited to a specific particle size. Mie theory, therefore, can be used for describing light scattering in a wide range of particles size, including Rayleigh particles [25]. Equation (2) is based on the electric dipole approximation and provides accurate results in the Rayleigh regime while for microparticles the ray-optics approximation must be used. On the other hand, the Mie cross section is obtained from a way more complicated than the Rayleigh

#175523 - $15.00 USD Received 5 Sep 2012; revised 15 Oct 2012; accepted 16 Oct 2012; published 8 Mar 2013

approximation. The details of its derivation are discussed in [28, 29]. The Mie scattering and extinction efficiencies are expressed as:

$$Q_{scat} = \frac{2}{x^2}\sum_{l=1}^{\infty}(2l+1)(|\,a_l\,|^2 + |\,b_l\,|^2), \tag{7}$$

$$Q_{ext} = \frac{2}{x^2}\sum_{l=1}^{\infty}(2l+1)Re(a_l + b_l), \tag{8}$$

with $x = kR$, where R is the particle radius. The efficiencies Q_i for the interaction of the radiation with a scattering particle of radius R are cross sections C_i normalized to the particle cross section, πR^2, where i stands for extinction ($i = ext$), absorption ($i = abs$) and scattering ($i = scat$), thus $Q_i = C_i/\pi R^2$. Energy conservation requires that $Q_{ext} = Q_{scat} + Q_{abs}$, or $C_{ext} = C_{scat} + C_{abs}$.

The coefficients a_l and b_l are given by:

$$a_l = \frac{\mu m^2 j_l(mx)\left[xj_l(x)\right]' - \mu_1 j_l(x)[mxj_l(mx)]'}{\mu m^2 j_l(mx)\left[xh_l^{(1)}(x)\right]' - \mu_1 h_l^{(1)}(x)[mxj_l(mx)]'}, \tag{9}$$

$$b_l = \frac{\mu_1 j_l(mx)\left[xj_l(x)\right]' - \mu j_l(x)[mxj_l(mx)]'}{\mu_1 j_l(mx)\left[xh_l^{(1)}(x)\right]' - \mu h_l^{(1)}(x)[mxj_l(mx)]'}, \tag{10}$$

where m is the refractive index of the particle relative to the host medium, the j_l's are spherical Bessel functions of the first kind, the h_l's are spherical Hankel functions, and μ_1, μ are the magnetic permeability of the particle and surrounding, respectively. For the present case no magnetic particles are considered, *i.e.* $\mu_1 = \mu$. A computer code to obtain C_{scat} and C_{abs} was developed by Christian Maetzler is readily available online [30]. Thus, gradient force for Rayleigh particle is calculated using Eq. (3) or the ray-optics approximation for microparticles while scattering and absorption forces for Mie particles are calculated by using Eqs. (4), (5), and Eqs. (7), (8). In order to evaluate the magnitude of the forces, several parameters must be calculated. The complex refractive index for zinc at 980 nm is $n_1 = 3 + 2.66i$ and its absorption coefficient is $\alpha = 4\pi\kappa/\lambda = 3.41\text{x}10^5$ cm^{-1} where $\kappa = 2.66$ is the zinc extinction coefficient [5], refractive index for isopropyl alcohol $n_2 = 1.36$, radius of the beam waist $w_0 = 4.1$ μm corresponding to the radius of a single-mode optical fiber, beam power $P = 5$ and 50 mW.

Figure 7 shows the longitudinal component of optical forces exerted on a zinc nanoparticle with a radius of 50 nm and considering a beam power of 50 mW. The fiber surface is located at $z = 0$. One can observe that gradient force (Fig. 7(a)), regardless of the particle size, is three orders of magnitude smaller than scattering/absorption forces (Fig. 7(b)) and therefore it can be neglected in the deposition mechanism.

Figure 8 shows the forces involved in the photodeposition process (scattering, absorption and Stokes) exerted on a zinc nanoparticle as a function of its radius for beam powers of 5 and 50 mW. Figure 8(a) shows both absorption and scattering forces when the nanoparticle is located near the fiber surface, where these forces take their maximum values as shown in Fig. 8(b), for two power values. These forces are always positive, meaning that the nanoparticle will move in the same direction as the beam propagation regardless of its size. Figure 8(b) shows that the Stokes force is negative for all nanoparticles, *i.e.* the particles will move towards the fiber surface. The net force that undergoes a zinc nanoparticle is given by the sum of these forces.

#175523 - $15.00 USD Received 5 Sep 2012; revised 15 Oct 2012; accepted 16 Oct 2012; published 8 Mar 2013

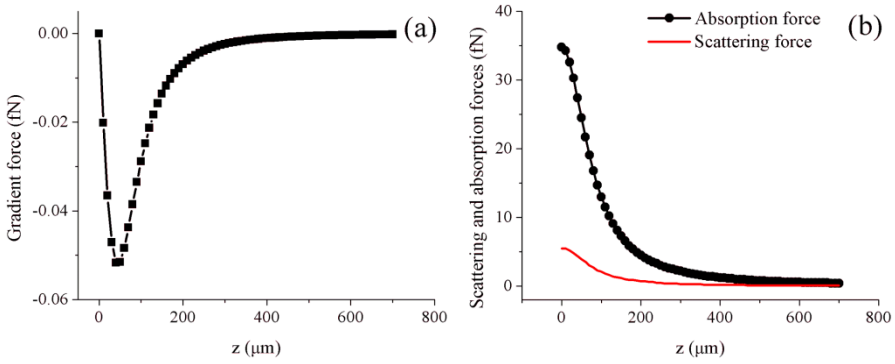

Fig. 7. Longitudinal component of optical forces exerted on a zinc nanoparticle (50 *nm*) in the photodeposition process as a function of *z* position. a) Gradient force, b) scattering and absorption forces.

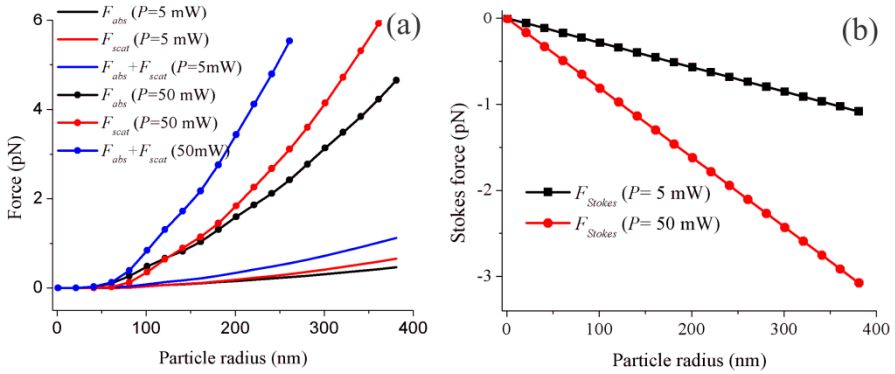

Fig. 8. Forces exerted on a zinc nanoparticle in the photodeposition process as a function of its size for two power beam (5 and 50 mW). a) Scattering and absorption forces when the nanoparticle is at position (0, 0, 0), b) Stokes force as a function of the particle radius.

Figure 9 shows the net force ($\boldsymbol{F}_{net} = \boldsymbol{F}_{abs} + \boldsymbol{F}_{scat} + \boldsymbol{F}_{Stokes}$) exerted on a zinc nanoparticle as a function of its radius for beam powers of 5 and 50 mW. When the beam power is 5 mW nanoparticles smaller than 361 nm will move towards the fiber end. Above this value the particles are forced to move along the beam direction. These means that particles with radius < 361 nm are more likely to deposit onto the optical fiber end. On the other hand, when the beam power is 50 mW, the size of the nanoparticles travelling towards the fiber end decreases to < 100 nm. The results of our simulations are in good agreement with our experimental results, as shown in Fig. 3. Therefore, it is possible to select the maximum radius of the collected nanoparticles by controlling the power of the beam.

The mechanism of particle deposition is a well-known phenomenon. Particles close to the core of the optical fiber end adhered to it because of particle interactions through a double layer repulsion and London attraction force [31]. If the beam power is large, the kinetic energy of the zinc particles outside the cone beam is very large and drags along the optical fiber and do not adhere to it (Figs. 3(d)-3(e)). However, when the beam power is smaller, its kinetic energy is also smaller and may adhere to the fiber core (Figs. 3(b)-3(c)).

The scattering and absorption forces depend on the particle position within the beam and reach their maximum when a particle is at the beam waist. Figure 9 shows that for a specific particle size, the optical forces are fully compensated by the Stokes force and therefore the particles should be trapped near the fiber end. In fact, Fig. 10 is a movie of particle trapping, where this condition is fulfilled. Although the trapping is not very stable, residence time is around two seconds with a beam power of 5 mW. Thus, a new mechanism of particle trapping

#175523 - $15.00 USD Received 5 Sep 2012; revised 15 Oct 2012; accepted 16 Oct 2012; published 8 Mar 2013

termed convective-optical trapping is demonstrated. The potential applications of this mechanism remain to be evaluated and it will be reported elsewhere.

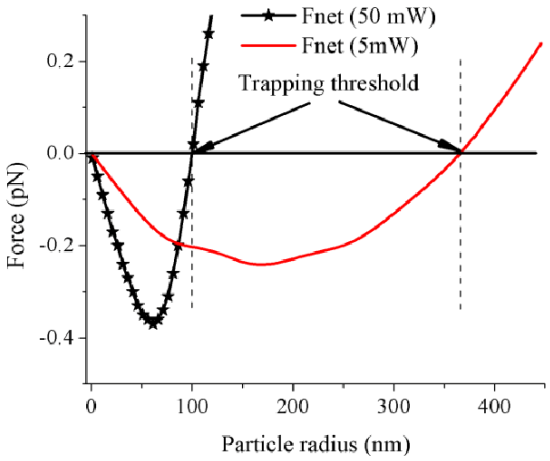

Fig. 9. Net force exerted on zinc nanoparticle in the photodeposition process as a function of its size for beam powers of 5 and 50 mW.

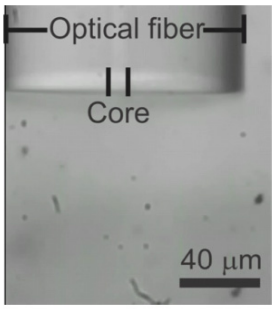

Fig. 10. Movie of convective-optical particle trapped by approximately two seconds (Media 2).

5. Conclusions

We demonstrated that photodeposition of metallic zinc nanoparticles on the core of the optical fiber is possible by a careful balance of the laser-induced convection flow and optical forces. The interplay of these forces produces a selective deposition that depends upon the size of the particles. The beam power is the key parameter to define the size of particles to be deposited on the fiber core. In addition, convective-optical trapping can be produced by an adequate balance of absorption, scattering, and Stokes forces. This simple and inexpensive method of deposition of metallic nanoparticles can be used in Raman sensors and saturable absorbers among others.

Acknowledgments

We appreciate the technical assistance of Miguel Galván Arellano and Adolfo Tavira Fuentes in the use of the X-ray diffractometer. This work was supported by CONACyT grant No. 130 983, Benemérita Universidad Autónoma de Puebla VIEP grant No. 339, and by PROMEP-Redes temáticas de colaboración 2008, "Fisioquímica de sistemas complejos nanoestructurados".

#175523 - $15.00 USD Received 5 Sep 2012; revised 15 Oct 2012; accepted 16 Oct 2012; published 8 Mar 2013